AFRL-RX-TY-TP-2008-4512

PREPRINT

FINITE ELEMENT ANALYSIS OF FLUID-STRUCTURE INTERACTION IN A BLAST-RESISTANT WINDOW SYSTEM

Jae H. Chung and Gary R. Consolazio
Department of Civil and Coastal Engineering
University of Florida
P.O. Box 116580
Gainesville, FL 32611

Robert J. Dinan and Stephen A. Rinehart
Air Force Research Laboratory

MARCH 2008

This document was submitted for publication in the American Society of Civil Engineers Journal of Structural Engineering.

AIRBASE TECHNOLOGIES DIVISION
MATERIALS AND MANUFACTURING DIRECTORATE
AIR FORCE RESEARCH LABORATORY
AIR FORCE MATERIEL COMMAND
139 BARNES DRIVE, SUITE 2
TYNDALL AIR FORCE BASE, FL 32403-5323

REPORT DOCUMENTATION PAGE

Form Approved
OMB No. 0704-0188

PLEASE DO NOT RETURN YOUR FORM TO THE ABOVE ADDRESS.

1. REPORT DATE *(DD-MM-YYYY)*	2. REPORT TYPE	3. DATES COVERED *(From - To)*
18-MAR-2008	Journal Article PREPRINT	01-OCT-2006 -- 31-DEC-2007

4. TITLE AND SUBTITLE

Finite Element Analysis of Fluid-Structure Interaction in a Blast-Resistant Window System

5a. CONTRACT NUMBER

FA4819-07-D-0001

5b. GRANT NUMBER

5c. PROGRAM ELEMENT NUMBER

62102F

6. AUTHOR(S)

Chung, Jae H.; Consolazio, Gary R.; Dinan, Robert J.; Rinehart, Stephen A.

5d. PROJECT NUMBER

4915

5e. TASK NUMBER

F2

5f. WORK UNIT NUMBER

Q210FA72

7. PERFORMING ORGANIZATION NAME(S) AND ADDRESS(ES)

Department of Civil and Coastal Engineering
University of Florida
P.O. Box 116580
Gainesville, FL 32611

8. PERFORMING ORGANIZATION REPORT NUMBER

9. SPONSORING/MONITORING AGENCY NAME(S) AND ADDRESS(ES)

Air Force Research Laboratory
Materials and Manufacturing Directorate
139 Barnes Drive, Suite 2
Tyndall Air Force Base, FL 32403-5323

10. SPONSOR/MONITOR'S ACRONYM(S)

AFRL/RXQF

11. SPONSOR/MONITOR'S REPORT NUMBER(S)

AFRL-RX-TY-TP-2008-4512

12. DISTRIBUTION/AVAILABILITY STATEMENT

Distribution Statement A: Approved for public release; distribution unlimited.

13. SUPPLEMENTARY NOTES

Submitted for publication in American Society of Civil Engineers Journal of Structural Engineering. Document contains color images.

14. ABSTRACT

This paper describes the development of a finite element model capable of representing a blast-resistant flexible window (flex-window) system developed by the Air Force Research Laboratory, Airbase Technologies Division (AFRL/RXQ). Computational fluid-structure interaction finite element simulations are used to develop an improved understanding of the manner in which fluid phenomena, such as air compression and flow, affect the behavior of the flex-window system under blast loading. Compressible air flow interacting with a flexible thin-shell structure of the flex-window (transient air-window panel interaction phenomena) is found to significantly influence system performance. The influences of shock wave propagation and fluid venting inside the damping chamber of the flex-window system are quantified and the influences of such phenomena on panel deflections, deformations, and internal forces are presented.

15. SUBJECT TERMS

blast loading, finite element method, dynamics response, computer models, fluid-structure interaction, full-scale tests

16. SECURITY CLASSIFICATION OF:			17. LIMITATION OF ABSTRACT	18. NUMBER OF PAGES	19a. NAME OF RESPONSIBLE PERSON
a. REPORT	b. ABSTRACT	c. THIS PAGE			Sheppard, Paul
U	U	U	UU	51	19b. TELEPHONE NUMBER *(Include area code)*

Reset

Standard Form 298 (Rev. 8/98)
Prescribed by ANSI Std. Z39.18

FINITE ELEMENT ANALYSIS OF FLUID-STRUCTURE INTERACTION IN A BLAST-RESISTANT WINDOW SYSTEM

Jae H. Chung[1] , Gary R. Consolazio[2] , Robert J. Dinan[3] and Stephen A. Rinehart[4]

Abstract

This paper describes the development of a finite element model capable of representing a blast-resistant flexible window (flex-window) system developed by the Air Force Research Laboratory (AFRL)/Airbase Technologies Division. Computational fluid-structure interaction finite element simulations are used to develop an improved understanding of the manner in which fluid phenomena, such as air compression and flow, affect the behavior of the flex-window system under blast loading. Compressible air flow interacting with a flexible thin-shell structure of the flex-window (transient air-window panel interaction phenomena) is found to significantly influence system performance. The influences of shock wave propagation and fluid venting inside the damping chamber of the flex-window system are quantified and the influences of such phenomena on panel deflections, deformations, and internal forces are presented.

CE Database Subject Headings

Blast loading, Finite element method, Dynamics response, Computer models, Fluid-structure interaction, Full-scale tests

[1] Research Assistant Professor, Department of Civil and Coastal Engineering, University of Florida, P.O. Box 116580, Gainesville, FL 32611

[2] [Corresponding author] Associate Professor, Department of Civil and Coastal Engineering, University of Florida, P.O. Box 116580, Gainesville, FL 32611; Phone (352)392-9537 Ext. 1510; Email: GRC@CE.UFL.EDU

[3] Chief, Engineering Mechanics and Explosive Effects Group, Air Force Research Laboratory, 104 Research Rd, Bldg 9742, Tyndall AFB, FL 32403

[4] Principal Staff Engineer, Air Force Research Laboratory, 104 Research Rd. Bldg 9742, Tyndall AFB, FL 32403

INTRODUCTION

Terrorist attacks during the past decade, both in the U.S. and worldwide, have highlighted the need for increased air-blast resistant designs in force protection against high profile targets such as embassies, mosques, airports, military personnel and civilian populations in crowded marketplaces. There can be severe damage caused by flying debris (i.e., glass shards resulted in over 80% of injuries and fatalities in the Oklahoma City attack of the Murrah Building) from explosive air-blast attacks by terrorists employing various Improvised Explosive Devices (IEDs). For the past decade, the U.S. Air Force Research Laboratory (AFRL)/Airbase Technologies Division has been involved in the development of innovative window systems capable of resisting combined air-blast loading and chem-bio attacks (Dover et al. 2002). Development of these blast resistant window systems has taken place in two distinct phases (or generations) of design, the first during the early 1990s, and the second more recently. Key issues addressed by the designs include resistance to initial blast loading and maintenance of window-seal integrity against subsequent chem-bio attack.

Prior to the development of blast resistant windows by the U.S. Department of Defense (DoD) and the State Department, the basic commercial (wind resistant) design procedure was to anchor a thick glass panel (0.75 to 1.5 in. thickness) between large window bites and then use high strength anchored films on the interior side of the window. The film is extended to the inside of the frame where it is either anchored or bolted with the intent of capturing flying glass shards. Both annealed and heat-tempered glasses are relatively brittle materials. Annealed glass (typically used in commercial applications) fails (breaks into shards) at 1.4 kPa (0.2 psi) and thermally tempered glass can fail at 6.9 kPa (1 psi). Wind resistant window designs are generally able to withstand approximately 69 kPa (10 psi) of reflected pressure in practice. However, the

threat level from an IED (e.g., a car bomb) can readily exceed 207+ kPa (30+ psi). Protection of government buildings may also involve the use of a continuous muntin steel tubing window frame anchored into a masonry wall with threaded rods to withstand the blast loads from an IED.

Among the varied window systems designed, fabricated, and blast-tested by the Air Force Research Laboratory (AFRL)/Airbase Technologies Division at Tyndall AFB, Florida, those incorporating an internal air-damping chamber (i.e., Flex window system) exhibited the best performance and greatest potential for application to larger surface-area applications. A comprehensive series of tests by AFRL have shown that the Flex window system is a dramatic improvement over existing commercially available blast-resistant windows because the most difficult issue of keeping the reinforced window from becoming a projectile has been successfully addressed. In these systems, composite glass and polymer (polyethylene terephthalate) film panels at the front and back of the window are anchored to a steel window frame using butyl rubber membranes, thus forming an internal air-filled damping chamber (Figure 1). Vent holes in the steel window frame regulate the rate of air flow out of the damping chamber as the blast wave deforms the front composite panel. Full-scale physical blast testing demonstrated that this type of system was capable of resisting very high blast pressures without suffering detectable breaching of the rubber window seal (Dover et al. 2002).

The process utilized by the AFRL to design the flex-window was based on engineering and mechanics principles, previous development experience, full-scale explosive testing, and engineering intuition. However, with only these tools available, multiple design iterations, fabrication, and blast testing were required to arrive at a successful design. Furthermore, design optimization—which requires that the sensitivity of system response to changes in key design parameters be evaluated—can be very costly using only full-scale explosive testing as the sole

validation method available. Evaluating the influence of window design parameters such as damping chamber volume and vent hole configuration is of particular interest here. Given the setup time and costs involved in full-scale explosive testing, conducting a strictly experimentally based parametric study to evaluate the influence of these parameters is cost prohibitive and would not be feasible.

As a consequence, in the study described here, steps were taken to develop an alternative methodology in which a portion of the conceptual design process could be performed using computational simulation (finite element analysis) rather than experimental testing (once the computational model was validated). Development of a finite element window model, and subsequent use of that model in a parametric sensitivity study were used to evaluate the influence of selected damping chamber characteristics. The AFRL second generation, anchor design No. 4, described by Dover et al. (2002), was chosen for the finite element model development. The University of Florida was given the task of determining whether the presence of the damping chamber was beneficial to the performance of the window system and if so, the extent to which window response was sensitive to changes in damping chamber characteristics (e.g. vent configuration and chamber volume). Selected numerical model validation procedures were carried to confirm that various components and aspects of the finite element model functioned properly and in accordance with relevant physics. Analysis of nonlinear dynamic structural response, fluid-structure interaction, and compressible fluid flow under blast loading conditions were carried out using LS-DYNA (version 970) (Hallquist 2003).

COMPUTATION OF BLAST LOADS

Data collected from full-scale explosive tests conducted by AFRL at Tyndall AFB on blast resistant engineering prototype window systems were used in this study. For each blast test

condition (defined by type of explosive, charge weight, and standoff distance), time-histories of reflected air-blast pressure and window deflection were measured by instruments attached to the window systems (Dover et al. 2002). Subsequently, air-blast calculation software was used to construct simplified time-histories of reflected pressure corresponding to the test conditions. After making minor adjustments to the charge size and standoff distance used in the simplified calculations, an acceptably close fit to observed test data was obtained. In Figure 2, typical sets of measured and calculated data are shown (note that the data have been normalized with respect to the peak numerically predicted pressure).

MODELING OF FLUID-STRUCTURE INTERACTION (FSI)

Finite element modeling of air flow, air compressibility, and fluid-structure interaction using LS-DYNA involves the development of Eulerian fluid meshes, equation of state descriptions, and definitions of interaction (contact) surfaces between fluid and structural elements. Fluid-structure interaction models typically consist of structural components meshed using Lagrangian solid and shell elements, and Eulerian fluid elements. In the Lagrangian formulation, the motions of nodes within the finite element mesh are tracked through space as the system deforms. This is in contrast to the Eulerian formulation in which the finite element mesh is constructed at a fixed position in space and the material of interest, typically a fluid, flows through the mesh. An Eulerian mesh thus serves as a fixed computational reference frame through which fluids flow (Belytchko et al. 2004).

In all of the models presented here, the solid fluid elements that discretize the flow domain for the fluid (i.e. air) make use of the LS-DYNA Eulerian element formulation referred to as “Eulerian single material and void.” Solid fluid elements formulated in this manner may be either fully occupied by a physical fluid (such as air), fully occupied by a computational void

(zero mass), or may contain a mixture of the two. In the case of a mixture, the material-to-void ratio within each element is quantified by a volume fraction parameter (Aquelet et al. 2003).

Fluid-structure coupling

Coupling between Lagrangian structural elements and Eulerian fluid elements in a fluid-structure interaction model is achieved using the LS-DYNA penalty coupling algorithm. For example, consider the conceptual model shown in Figure 3. An Eulerian material such as air residing inside the chamber undergoes a prescribed time-varying volumetric change that results from movement of a structural (Lagrangian) plate. A Fluid Structure Interaction (FSI) contact definition between the plate and the fluid, in which relative displacements between the Lagrangian nodes and the Eulerian material are computed using a penalty coupling algorithm (Souli et al. 2004), forces the air to be contained within a chamber volume that first contracts and later expands. During the contraction stage, air flows through the spatially-fixed Eulerian mesh into a chamber volume that continues to decrease with movement of the plate. Fluid elements that are initially filled with air transition to void elements once the structural plate passes through. Due to the reduction of chamber volume, the air undergoes an increase in pressure which in turn exerts a pressure load on the structural plate (i.e., window glass). When the motion of the plate is reversed, void elements in the Eulerian mesh serve as a computational framework into which the air may once again flow as the volume of the chamber increases.

Equation of State (EOS)

The air model used in this study is a linear polynomial representation that models pressure dependent thermodynamic states for perfect gases. The air is assumed to be an ideal (perfect) gas with neither shearing nor frictional forces acting between its particles. Thus, the Gamma Law Equation of state can be employed to prescribe the boundary and initial

thermodynamic conditions of air in the model (Kuethe and Chow 1986). Therefore, the air pressure inside the chamber is determined by a linear polynomial function—specifically, a function of the ratio of specific heats γ, mass density ratio η, and specific internal energy per specific volume e that relates pressure to other state variables as:

$$P = C_0 + C_1\mu + C_2\mu^2 + C_3\mu^3 + (C_4 + C_5\mu + C_6\mu^2)e \quad (1)$$

In this expression, P represents absolute pressure, the coefficients C come from data fitting or derivations based on thermodynamics, and μ is a volumetric parameter determined by γ and η as (Shapiro 1953):

$$\mu = (\gamma - 1)\eta = (\gamma - 1)\frac{\rho_{current}}{\rho_{initial}} \quad (2)$$

Here, $\rho_{current}$ and $\rho_{initial}$ represent current mass density and initial mass density, respectively. Usually, setting the pressure alone is not sufficient to provide a determinate state for boundary or initial conditions. If the material will not undergo chemical reactions or phase change, then two more thermodynamic variables, such as specific volume ratio and specific internal energy, may be used to complete the description of boundary or initial conditions. With a known initial pressure, the necessary values of γ and η may be back-calculated via the EOS in order to set up the boundary and initial conditions. For example, parameters of the linear polynomial material model can be selected to produce 1 atm of pressure (0.1013 MPa) as an initial pressure by setting the coefficients to $C_0 = C_1 = C_2 = C_3 = C_6 = 0$ and $C_4 = C_5 = \gamma - 1 = 0.4$ for a perfect gas. As described by Hallquist (2003), C_0 may also be used to set the initial pressure. However, setting $C_0 = 0$ does not necessarily mean that the initial pressure is zero. The initial pressure depends also on the initial value μ_i, which is equal to 0.4, and e_i, the initial specific internal energy per

specific volume, which for standard atmospheric pressure is equal to $e_i = P_i / \mu_i$ = 0.1013/0.4 = 0.25325 MJ/m^3. These values were selected to initialize the thermodynamic state of the finite element models presented in this paper. Air material parameters are given in Table 1.

Fluid-structure interaction (FSI) verification analyses

Two fluid-structure interaction analyses are presented here for the purpose of verifying proper functioning of the selected fluid-structure coupling algorithm and the air equation of state and material parameters. In each analysis, heat flow between the fluid and the surrounding system is omitted and fluid temperature change due to the work done by the system is assumed to be negligible. Hence, although the analyses involve volume, pressure, density, and energy changes, as well as mass flow, they are non-thermal in nature.

Compression of a perfect gas in thermal equilibrium

The first verification case consists of an enclosed box filled with air (Figure 4-a). A moveable plate spanning the cross-sectional area of the box is displaced in such a manner as to alter the volume occupied by the air. As the plate moves downward, the volume of air enclosed in the box is decreased and the air is compressed. The only interaction permitted between the system and its environment is the performance of work done to the system, i.e., compression of the air.

The compressibility of the air is expressed as an extension of the conservation of energy principle with inclusion of thermodynamic system changes:

$$\Delta U = U_f - U_i = Q - W \tag{3}$$

where ΔU is the change of internal energy, U_i is the initial internal energy, U_f is the final internal energy (after completion of the compression process), Q is the heat inflow, and W is the

work done. Since heat flow between the fluid and the surrounding system is assumed to be negligible (and is therefore is omitted from the analysis), $Q = 0$ and ΔU becomes:

$$\Delta U = -W \tag{4}$$

Eqn. (4) indicates that if W is positive (work is done by the system), there must be a decrease in the internal energy. Conversely, if W is negative (work is done on the system), there must be an increase in the internal energy. For a differentially small displacement ds of the plate, the work done on the system dW is:

$$dW = F \cdot ds = (P \cdot A) \cdot ds = P \cdot (A \cdot ds) = P \cdot dV \tag{5}$$

where A is the surface area of the plate in contact with air. Eqn. (5) states that the product of exerted force F and the downward plate movement ds is equal to the product of pressure P and volume change dV of the air. Therefore, the total work done during a finite displacement of the plate is given by:

$$W = \int dW = \int_{V_i}^{V_f} P\, dV \tag{6}$$

In its initial state, the air in the system shown in Figure 4-a has a volume equal to 50,000 mm^3. Assuming an initial pressure equal to 0.1013 MPa and using the air equation of state described earlier, the initial internal energy per unit reference specific volume e_i is equal to 0.25325 MJ/m^3. The initial internal energy of the system may then be calculated as the product of e_i and the initial volume V_i:

$$U_i = e_i \cdot V_i \tag{7}$$

For the initial state of the system, a theoretical value of the internal energy $U_i = (0.25325\ \text{MJ/m}^3)(50{,}000\ \text{mm}^3) \approx 12.66\ \text{J}$ matches the initial condition indicated by the finite element analysis results (Figure 4-b).

With the mass of the air held constant and thermal changes omitted, the plate in the finite element model is moved downward a distance of 50 mm over a time span ranging from t=0 sec to t=0.1 sec, producing a total volume decrease of 25,000 mm^3. The position of the plate is assumed to be held constant from t=0.1 sec to t=0.5 sec. The resulting change in the internal energy of the system can be computed from Eqns. (1), (4) and (6):

$$\begin{aligned} \Delta U &= -W = -\int_{V_i}^{V_f} P\, dV \\ &= -\int_{V_i}^{V_f} (\gamma - 1)\frac{\rho}{\rho_i} e_i\, dV = (1-\gamma) V_i e_i \int_{V_i}^{V_f} \frac{1}{V} dV = (1-\gamma) V_i e_i \ln\left(\frac{V_f}{V_i}\right) \end{aligned} \tag{8}$$

Using Eqn.(8), the change of internal energy of the system is equal to $\Delta U = -W = (1\text{-}1.4)(50{,}000\ \text{mm}^3)(0.25325\ \text{MJ/m}^3)\ ln(0.5) \approx 3.51\ \text{J}$. The total internal energy of the system is then given by the initial energy plus the change:

$$U_f = U_i + \Delta U \tag{9}$$

and is equal to U_f=12.66 J + 3.51 J=16.17 J. Results obtained from the finite element analysis at points in time after the compression process has completed (Figure 4-b) agree with this value to within a small margin of error (approx. 3% at t=0.5 sec). It is noted that kinetic energy K of the air (attributable to mass inertial effects) produces a slight increase in the total system energy E_{total} in comparison to the internal energy. Considering the contribution of kinetic energy to the total system energy, $E_{total} = U_f + K = U_i - W + K$, the finite analysis results are seen to obey the first law of thermodynamics.

In addition to energy considerations, the pressure-volume relationship for the compression process is also satisfied by the finite element simulation. Given that the air undergoes a volume reduction of 50% without a change of temperature, the final system pressure will be equal to twice the initial pressure, $P_f = 2P_i$ = 2 (0.1013 MPa) = 0.2026 MPa. Examination of the pressures predicted by the finite element analysis throughout the model averaged 0.1992 MPa at t=0.5 sec indicating good agreement with the expected pressure-volume relationship.

In conducting this finite element simulation, numerical viscous hourglass control (Hallquist 2003) had to be employed to prevent computational instabilities from occurring in the under-integrated fluid finite element mesh. In addition, the coarse mesh resolution used to model the rigid plate caused a small quantity of fluid leakage from the volume being compressed. The small amount of dissipated internal energy was found to contribute to the numerical errors observed.

Simulation of free expansion

In this verification case, free expansion and flow of air from one chamber to another is simulated. As shown in Figure 5-a, two chambers each 100 mm x 100 mm x 5 mm in size are connected together. The left chamber is filled with air that is maintained at a constant pressure of 0.1013 MPa (the constant pressure condition is modeled using the LS-DYNA Eulerian ambient element formulation). Initially, the right chamber is in a vacuum condition and flow between the chambers is prevented by a valve that is modeled using rigid plate elements. The expansion and flow processes consist of opening the valve (by displacing the valve plate) and then allowing the system to come to equilibrium. When the system reaches the equilibrium state, air occupies both chambers at a constant pressure of 0.1013 MPa. No heat transfer occurs in the simulation. No

work is done because, as the expanding air flows into the vacuum, its motion is unopposed by any countering pressure. The external work done on the system is therefore zero: $-W = 0$.

Since the volume of air in the system doubles while maintaining a constant pressure, the total energy of the system at the final equilibrium state must be twice that of the initial state:

$$U_f = U_i + \Delta U = (P \cdot V_i) + (P \cdot \Delta V) = (P \cdot V_i) + (P \cdot V_i) = 2\,P \cdot V_i = 2 \cdot U_i \qquad (10)$$

Using Eqn. (10), the final energy content of the dual chamber system is found to be $U_f = 2 \cdot U_i = 2 \cdot 12.66$ J =25.32 J. As Figure 5-b demonstrates, the finite element simulation results agree well with this theoretical value.

FINITE ELEMENT WINDOW MODEL

To facilitate numerical assessment of whether window performance is substantially affected by fluid-related design features—e.g. air damping chambers and vent holes—a finite element model of the AFRL flex-window is developed. A summary of the key components of the finite element window model is provided in Table 2 together with corresponding element types and material models. Due to symmetry of the structural configuration, symmetry of the venting, and symmetry of the imposed blast loading, only one-quarter of the overall window is modeled for simulation purposes (Figure 6).

Modeling fluid flow and fluid-structure interaction

Fluid components of the model include air enclosed within the damping chamber and air surrounding the vented window frame. Air inside the window chamber is modeled in such a way as to allow both compressibility and flow while air outside the window is modeled as an atmospheric fluid that remains at constant pressure. To ensure that air-flow out of the chamber occurs only through vent holes in the window frame, no-flux boundary conditions are imposed

along each of the symmetry planes that cut through the window's internal chamber. Fluid-structure contact definitions are used to model interaction (load transfer) between the window panels and the enclosed air. As the imposed blast pressure deforms the front panel into the damping chamber, an internal shock wave is generated inside the enclosed air volume which, in turn, transfers load to the rear panel.

Fluid (air) in the window model is divided into five basic zones (Figure 6a), each of which is discretized into a mesh of solid fluid elements. All air elements considered in this study make use of the LS-DYNA Eulerian "single material and void" element formulation. Initial pressures in zones 1, 2, and 3 are set at standard atmospheric pressure (0.1013 MPa) through selection of the terms in the `*EOS_LINEAR_POLYNOMIAL` equation of state, as described earlier.

Fluid zones 1, 2, and 3—the internal damping chamber, the lateral atmospheric chamber, and the vertical atmospheric chamber—are connected together via cylindrical meshes of the vent holes such that air may flow between them. By merging the damping chamber mesh, the atmospheric chamber meshes, and the cylindrical vent meshes, a continuous Eulerian flow domain is established. Representing constant pressure conditions in the lateral and vertical atmospheric chambers is achieved by making their volumes very large relative to that of the internal damping chamber.

Fluid-structure interaction (FSI) between the front and rear window panels and air in the damping chamber is achieved using the coupling algorithm `*CONSTRAINED_LAGRANGE_-IN_SOLID`. As the front window panel deforms in response to applied blast pressure and passes through elements in the Eulerian mesh, air in the damping chamber is forced to flow through the solid fluid elements and over-pressures are generated. These pressures generate loads that are applied to the inside surfaces of the front and rear window panels (Lagrangian structural

components of the model). Due to the sealed nature of the glass window panels and the butyl rubber membranes (Figure 6-b), air initially residing inside the damping chamber does not flow across the FSI boundaries formed by the Lagrangian structural mesh.

At front and rear of the window are two additional Eulerian zones (Figure 6a). These exist solely to serve as computational frameworks into which air inside the damping chamber may move as the front and rear window panels flex. Atmospheric pressure acting on the outside surfaces of the front and rear window panels is not modeled with fluid elements, but is represented by applying constant (spatially as well as temporally) pressure loads of 0.1013 MPa to these surfaces. Overpressure associated the blast loading is then superimposed on the atmospheric pressure that acts on the front window panel. In the absence of a blast overpressure, the external atmospheric 0.1013 MPa pressures satisfy static equilibrium with the initial internal damping chamber pressure (also at 0.1013 MPa (14.7 psi)) that is generated through specification of EOS parameters.

Modeling the window anchorage system

Due to the large stiffness of the outer steel window frame, and because the structural response of the frame is not a focus here, a rigid material property is used to model its behavior. Solid elements are used to discretize the geometry of the frame and the vent holes that permit air to flow from inside the damping chamber out to the atmosphere surrounding the window frame. Outer surfaces of solid elements in the frame mesh form two of the boundary planes that enclose the air volume inside the window.

Each window panel, located in both the front and rear portions, is anchored to the steel frame via a butyl rubber membrane. Constitutive behavior of the rubber is represented using the Blatz-Ko material model which is capable of modeling nearly incompressible behavior. Layering

of the structural components used to anchor the window panels to the frame is illustrated in Figure 6-b.

In the physical window system, the rubber membranes are sandwiched between layers of steel and glass and are fastened to both the window frame and the window panels via automotive-glass adhesive and steel bolts. Approximate numerical modeling of this anchorage is accomplished using tied contact surfaces (Figure 7). Each tied contact surface generates a set of constraint equations that mathematically link two surfaces together at their common interface to achieve compatibility in the deformations. Parts linked together in this manner may still deform and respond to load, as may the interface between them, but the surfaces of the two parts remain linked to each other on a point-by-point (or node-by-node) basis.

Modeling the window panels (Lessons Learned)

Each panel (front and back) in the window is a composite structure formed by sandwiching and bonding a single pane of tempered glass between two thin polymer films. When subjected to blast loading, the tempered glass pane fragments into a multitude of small pieces that remain confined between the film layers. This inelastic deformation mode is often referred to as *marbleization* based on the visual appearance that the panel takes on after fragmentation has occurred (Conrath et al. 1999). When designed to have sufficient strength, the polymer films remain structurally intact and contribute significant membrane (in-plane axial) stiffness to the overall behavior of the window panel, even after marbleization of the glass has occurred.

Considering the physical layering of the window panel constituents, the initial approach taken in modeling the panels involved the use of multiple, discrete layers of shell elements in which each layer represented the properties of either glass or polymer film (Du Bois et al. 2003). An approximate means of accounting for panel marbleization was attempted through the use of a

glass material model that permitted specification of a failure strain limit. Blast simulations performed using this modeling technique were unfortunately found to be problematic in that severe "hourglassing" was observed in the shell elements making up the glass layer. As a consequence, energy was numerically (rather than physically) dissipated, and the dynamic time-stepping process became unstable leading to termination of the simulation or unreliable analysis results.

Proposed Solution for Hourglassing

Problems associated with element hourglassing (Consolazio et al. 2003) can often be remedied by using fully integrated element formulations or by invoking special hourglass-energy control techniques (Bathe 1996) (e.g. the use of artificial viscous damping). In the present study, however, neither of these measures was sufficient to eliminate the hourglass mesh instabilities. Due to the order of magnitude differences in stiffness and thickness of the glass pane and the thin polymer films, abrupt deletion of failed glass shell elements generated abrupt redistributions of in-plane stress that subsequently initiated mesh instabilities. Reduction of hourglass instabilities to an acceptable level (quantified by maintaining the hourglass energy at less than 1% of total system energy) was ultimately achieved, not only by using fully integrated elements and hourglass control algorithms, but also by significantly increasing the resolution of the finite element mesh. In total, approximately 1,000,000 elements per panel were necessary to ensure solution stability. By reducing the sizes of the glass pane elements, the magnitudes of stress redistributions caused by element deletions remained at an acceptably low level and prevented instabilities. However, while stable solutions were obtained, the very high-resolution mesh was deemed to be impractical from the standpoint of conducting a parametric study involving numerous repeated simulations.

An alternative, more numerically efficient solution was achieved by abandoning the approach of modeling the glass and polymer layers using separate elements. Instead, the composite through-thickness structure of the window panel was modeled using the LS-DYNA material model `*MAT_LAMINATED_GLASS`. This material model uses multiple through-thickness integration points to account for layers of glass and polymer within a *single* shell element. For the composite glass panels of interest here, in which a central core of glass is sandwiched between two polymer films, two through-thickness integration points were used to represent the glass core, thus dividing it into two logical sub-layers. For each of these glass sub-layers, a failure strain limit was specified, as before.

In this laminated model, determination of glass failure is carried out on a sub-layer-by-sub-layer and integration-point-by-integration-point basis. That is, strain at each integration point in the 2 by 2 pattern used per logical sub-layer is evaluated (Figure 8). This process is then repeated for each glass sub-layer within the element. When exceedance of the failure strain occurs at an integration point in a glass sub-layer, neither the entire element nor the entire sub-layer is deleted. Instead, the contribution to overall element stiffness due to that single integration point is lost and there is a redistribution of internal stress to the remaining glass and polymer sub-layers. In contrast to the all-or-nothing element deletion approach of the previous modeling technique, this approach leads to a more controlled and gradual redistribution of internal stresses as the glass fails, thus permitting stable solutions to be obtained at coarser levels of mesh resolution (approximately 125,000 elements per panel). Due to the robustness and increased numerical efficiency of this latter modeling technique, it was used throughout the remainder of the study.

Modeling air blast loading

A review of the AFRL flex-window full-scale explosive blast test data was conducted to identify a representative loading condition in terms of charge size, standoff, and pressure. The selected condition corresponded to the physical blast under which the AFRL second generation anchor design number 4 (Dover et al. 2002) was tested. For this condition, a simplified time-history of reflected pressure was constructed using air-blast calculation software, as discussed earlier. It was assumed that the blast pressure could be taken as spatially uniform over the entire surface of the front window panel (Beshara 1994). Loading of the finite element model was achieved by prescribing time-histories of surface overpressure loading for each of the shell elements in the front window panel. In the simplified blast calculations, time $t = 0$ was taken as the instant at which explosion occurred. In contrast, in the finite element simulations, time $t = 0$ was taken as the instant at which the blast wave arrived at the front window panel. Hence, the pressure time history used in the LS-DYNA simulations was generated by time-shifting the simplified data so that the peak reflected blast pressure occurred at time $t = 0$, as shown in Figure 9.

SIMULATION OF THE AFRL FLEX WINDOW

Using the modeling procedures described above, finite element simulations are used to evaluate both structural and fluid responses of the AFRL flex-window system under representative air blast loadings from an IED.

Assessment of window panel response

For the purpose of assessing window panel deflections generated by exposure to blast pressure, two contrasting simulation cases are performed. The first consists of a “structure-only” simulation in which all fluid-structure interaction effects are excluded by omitting Eulerian fluid

elements from the model and retaining only Lagrangian structural elements. Subsequent to this case, a second—and more accurate—simulation is conducted in which fluid-structure interaction effects are included. Conducting the initial structure-only simulation permits verification that contact detection between the front and rear panels is functioning properly. By omitting air from the damping chamber, load transfer from the front panel to rear panel can *only* take place through direct contact. More importantly, however, results obtained from the structure-only simulation serve as baseline response data to which FSI simulation results may be compared in order to assess the effects of air compressibility and flow.

Deflection results obtained for the front and rear panels using the structure-only blast simulation are shown in Figure 10. Without development of air pressure on the rear face of the front panel (due to the lack of fluid effects), the only sources of resistance to deflection are those related to structural stiffness and inertial (mass-related) resistance. Given the limited cross-sectional panel thickness, the majority of structural stiffness in each panel is associated not with flexure but with membrane effects that only become significant at large out-of-plane deflection levels (Ugural 1981). Similarly, the mass of each panel, and therefore the inertial resistance, is relatively small in comparison to the magnitude of blast pressure applied. Consequently, the front window panel has very little initial (zero-deflection) resistance and rapidly deflects inward in response to applied blast loading. Within 5 msec after the air blast wave arrival, the front window panel undergoes sufficient inward deflection to directly contact the rear window panel. Prior to this contact event, the rear panel is in an unloaded state. Once contact occurs however, the front panel exerts a contact load on the rear panel and both deflect dynamically. As out-of-plane deflections grow, so do the panel in-plane membrane forces. Eventually the membrane stiffness halts deflection and the panels rebound. Results from the simulation indicate that

exceedance of glass-pane failure strains occurs in both front and rear panels, suggesting panel marbleization has taken place.

Assessing the influence of fluid effects on the performance of the window is carried out by conducting a more detailed FSI simulation. Results are illustrated in Figure 11. In this simulation case, air compressibility, air flow, and fluid-structure interaction effects are taken into account. Responding to the applied external blast load, the front window panel rapidly deflects into the damping chamber, producing a decrease in chamber volume and an increase in internal air pressure. This increase in pressure generates a fluid "cushioning" effect on the front panel in which air-pressure resistance adds to the structural and inertial resistances of the panel. Consequently, front panel deflections predicted by the FSI simulation are significantly less than those predicted by the earlier structure-only simulation.

In Figure 12, deflections predicted by FSI and structure-only simulations at two points on the front and rear panels are compared. As Figure 12-a illustrates, the maximum deflection of the front panel center point (location A-2) predicted by FSI simulation (81 mm (3.2 in.) is only one third of that predicted by structure-only simulation (244 mm (9.6 in.)). Thus, the effect of fluid resistance on deflection of the front panel is significant. In Figure 12-b, rear panel deflections predicted by structure-only and FSI simulation are compared. At the center point of the rear panel (location B-2), the maximum magnitudes of deflections in both cases are nearly equal (120 mm (4.75 in.)). However, the time durations required to achieve maximum deflections are different: rear panel motion in the FSI simulation occurs at a later point in time than in the structure-only case.

Assessment of damping chamber air pressure

Results from the FSI simulation demonstrate that fluid effects strongly influence the dynamic responses of both front and rear panels in the AFRL flex-window system. Hence, it is desirable to investigate the fluid related load transfer mechanism in additional detail, and to compare pressures numerically predicted inside the damping chamber with pressure data experimentally measured during physical blast testing of the AFRL flex-window system.

In the full-scale AFRL explosive air blast tests conducted, pressure transducers were installed in front of, inside, and behind the flex-window system. Gauge pressures (overpressures) measured by these devices were sampled and recorded at very high speed during each test. Pressure data measured by the transducer at the front of the window were used to determine the blast wave arrival time relative to charge detonation. This value was used to time-shift the pressure data collected by the transducer inside the window so that the new time origin ($t = 0$) for the latter device corresponded to the arrival of the blast wave at the front window panel—thereby matching the time origin of the numeric simulations.

To facilitate a comparison between simulation-predicted air pressure results and experimentally collected data, three locations within the spatially fixed Eulerian fluid mesh are examined (Figure 13-a). At each location (A, B, and C), pressure data for the two Eulerian elements nearest the damping chamber centerline (Figure 13-b) are averaged to produce a single "centerline" pressure time history. Since pressure results obtained from the numeric simulation process are absolute pressures, standard atmospheric pressure (0.1013 MPa (14.7 psi)) is subtracted from the simulation data to yield predictions of internal chamber overpressures. In Figure 14, simulation and experimental data are compared. The simulation pressures are generally of the same order of magnitude and duration as those measured experimentally, indicating agreement. Time-to-peak differences observed are likely due to differences in

through-thickness sampling location within the damping chamber. Placement of the experimental transducer nearer to the front panel than to the centerline of the chamber would result in a more rapid experimentally measured pressure rise, as indicated by experimental data in Figure 14.

DESIGN-PARAMETER SENSITIVITY STUDY

FSI simulation results presented above demonstrate that fluid effects such as air compressibility and direction of the flow may have beneficial influence on system performance. Of particular interest in assessing the performance of the AFRL flex-window system is the structural loading (internal force) imposed on the rear rubber membrane that ties the rear window panel to the window frame. A decrease in structural loading on this component represents an increase in the probability that an un-breached chemical/biological seal will remain intact after the blast event is complete. For the rear rubber membrane, total structural loading is a function both of the local air pressure near the boundary of the window as well as reaction forces that arise in anchoring the window panels as they dynamically deflect outward. The fact that air flow through vent holes decreases the local air pressure near the boundaries of the window (i.e., near the rubber membrane) is an indication that inclusion of such design features is beneficial to improving the survivability of the window. Thus, relieving pressure development in a regulated manner through inclusion of vent holes can reduce the structural demand on key system components such as the anchor membranes. In order to quantify such effects, a parametric study is conducted to evaluate the sensitivity of system performance to two primary design parameters: *i*) vent hole diameter, and *ii*) damping chamber thickness.

Elongation of the rear membrane

A total of seven separate window models are analyzed (Table 3)—the AFRL FSI model described above plus six new models. Since ensuring the survivability of the flex-window system

against combined chemical/biological threats is an important design consideration, investigating the deformation of the rear membrane is a suitable assessment process. Elongations are computed along a line where the most severe deformations are likely to occur: line A-B shown in Figure 15.

As Table 3 indicates, the T6 set of simulations all make use of a fixed chamber thickness of 152 mm (6 in.)—the thickness of the AFRL flex-window. The initial case (D0/T6) utilizes an un-vented (completely sealed) damping chamber. The remaining T6 cases (D0.75/T6 through D4/T6) utilize vent hole diameters ranging from 19 mm (0.75 in.) to 102 mm (4.0 in.). Two additional T10 simulations are also conducted that make use of a damping chamber 254 mm (10 in.) in thickness. Vent hole configurations considered for the T10 cases include the AFRL vent hole diameter (D1.5/T10) and a 102 mm (4 in.) vent diameter (D4/T10).

For comparison, total elongation (change of length) results of the rear anchor membrane for each of the window systems cited in Table 3 are normalized by the result from the baseline AFRL D1.5/T6 case and presented in Figure 16. Rear rubber membrane elongation data for the T6 cases exhibit only minimal sensitivity to vent hole diameter. In contrast, results obtained from the T10 simulations suggest that increasing the damping chamber thickness decreases the elongation of the membrane and might therefore offer promise as a design modification.

Further examination of the T10 results also reveals that the relationship between damping chamber volume, vent area, and structural demand is not as simple as might be intuitively expected. Instead, it is apparent that an “optimal” design must balance the interacting influences of various system parameters. For example, the most effective of the seven systems studied here appears to be the D1.5/T10 case that uses an increased chamber thickness of 254 mm (10 in.) but the same 38 mm (1.5 in.) diameter vent holes that are used in the baseline AFRL D1.5/T6 design.

Simply maximizing (or minimizing) vent size and/or chamber size does not produce an optimal design.

Resultant force of the rear membrane

In order to provide an additional index of structural demand on the rear membrane, supplementary calculations are performed for a subset of the simulations listed in Table 3. For the baseline AFRL D1.5/T6 window, the un-vented D0/T6 window, and the "optimal" D1.5/T10 window, transverse shear forces and resultant reaction forces acting along the perimeter of the rear membrane are computed. Since a key role of the rear membrane is to anchor the rear window panel to the frame, quantifying these forces provides an alternative means of comparing relative system performance and evaluating the loads that would be imparted to the surrounding wall system.

In Table 4, maximum relative shear and resultant anchorage forces for the D0/T6 and D1.5/T10 cases are compared to results obtained from the baseline AFRL D1.5/T6 simulation. Elongation data plotted earlier in Figure 16 for the un-vented D0/T6 case differed only moderately from the AFRL D1.5/T6 data. However, as Table 4 indicates, the maximum generated anchorage forces (shear and resultant) for these two cases differ substantially. When venting is eliminated and a sealed chamber is used, internal air pressures developed near the perimeter of the window (e.g., near the rear rubber membrane) are not dissipated as they are in a vented system. As a result, the influence of local air pressure substantially increases the structural loading on the rubber membrane. Thus, although the elongation data plotted in Figure 16 for line A-B (Figure 15) indicate only moderate sensitivity to venting characteristics, more global measures of structural demand, such as the relative forces presented in Table 4, indicate that benefit is derived from inclusion of venting.

With regard to performance of the D1.5/T10 system versus the baseline AFRL D1.5/T6 system, relative force data presented in Table 4 generally agree with the trends in elongation data shown in Figure 16. Both sets of comparisons suggest that an improved design might be achieved by increasing the damping chamber thickness and simultaneously determining a corresponding optimal vent diameter.

SUMMARY AND CONCLUSIONS

In this study, computational fluid-structure interaction (FSI) finite element simulations have been used to develop a much improved understanding of the dynamic coupled fluid-structure interactions and the manner in which fluid affects the behavior of the AFRL flex-window system under full-scale explosive air blast loading. Components of the study have included *i*) development of representative blast-loading pressure time-histories; *ii*) development of fluid-structure interaction models of the AFRL flex-window system; *iii*) simulation of flex-window response to blast loading both with and without fluid effects included; *iv*) investigation of system performance sensitivity to variations in vent size and chamber size; and *v*) evaluations of representative system performance indices including air pressures, elongation deformations, deflections, and internal forces. The AFRL flex-window system design that proved acceptable included front and rear glazings fabricated with annealed glass with rubber sheets that extend into the bite. The glass and rubber are the same thickness and are connected using PET film on each side. The damping chamber space between the window panes may be 127 mm (5 in.) to 178 mm (7 in.) which is approximately the width of a CMU block. However, the simulations show that increasing the damping chamber thickness (say to 254 mm (10 in.)) while simultaneously determining a corresponding optimal vent diameter (38 mm (1.5 in.) diameter)

could further reduce the maximum membrane shear forces (by > 30%) as well reduce the resultant force.

An important area of focus here was the development of numerical descriptions of interface boundaries between compressible air in the damping chamber and structural components of the AFRL flex-window system. Specifically, the study focused on the development of a robust computational model capable of adequately simulating transient fluid-structure (air-panel) interaction phenomena.

The influences of shock wave propagation and fluid venting inside the damping chamber have been quantified and the influences of such phenomena on panel deflections, deformations, and internal forces have been studied. It has been determined that inclusion of vents reduces localized air pressure development in the vicinity of the rubber anchor membranes and thus reduces the total structural demand imposed on these critical structural components. Failure to incorporate vents results in the development of substantial air pressures that increase total structural demand on the rubber anchor membranes. Sensitivity study results revealed that increasing the thickness (and therefore volume) of the damping chamber while maintaining a properly selected vent configuration offers the promise of potentially improved flex-window performance. Generally, it has been determined that optimal design of a system involving fluid structure interaction, shock wave propagation, and fluid flow requires careful balancing of the influences of multiple design parameters; simply maximizing or minimizing selected parameters without adequately evaluating how these parameters interact will generally not lead to optimal system performance.

ACKNOWLEDGEMENTS

This study was made possible by research funding provided by the Research Laboratory at Tyndall/Airbase Technologies Division under contract BAA-TYN-03-001. Suggestions provided by Dr. Ian Do, of Livermore Software Technology Corporation, regarding analysis of fluid-structure interaction are also appreciated.

REFERENCES

Aquelet, N., Souli, M., Gabrys, J., Olovson, L. (2003). "A New ALE Formulation for Sloshing Analysis." Structural Engineering and Mechanics, 16(4), 423-440.

Bathe, K.J. (1996) *Finite Element Procedures*, Prentice Hall, Upper Saddle River, New Jersey.

Belytchko, T., Liu, W.K., Moran, B. (2004). *Nonlinear Finite Elements for Continua and Structures*, Wiley, New York.

Beshara, F.B.A. (1994). "Modeling of blast loading on above ground structures I: General Phenomenology and External Blast." *Computers and Structures,* 51(5), 585-597.

Conrath, E.J., Krauthammer, T., Marchand, K.A., Mlakar, P.F. (1999). *Structural Design for Physical Security*, SEI Publication, ASCE, Reston, VA.

Consolazio, G.R., Chung, J.H., Gurley, K.R., (2003). "Impact Simulation and Full Scale Crash Testing of a Low Profile Concrete Work Zone Barrier." *Computers and Structures*, 81(13), 1359-1374.

Dover, D., Anderson, M., Vickers, R.N. (2002). "Sealed Window Glazing System for Chemical Biological Protected Space Applications", Proc., Nuclear Biological Chemical Defense Collective Protection Conference (COLPRO 02), Orlando, FL.

Du Bois, P.A., Kolling, S., Fassnacht, W. (2003). "Modeling of safety glass for crash simulation." Computational Material Science, 28, 675-683.

Hallquist, J.O. (2003). LS-DYNA Version 970 Theoretical manual, Livermore Software Technology Corporation, Livermore, CA.

Kuethe, A.M., Chow, C. (1986). *Foundations of Aerodynamics: Bases of Aerodynamic Design*, 4th ed., Wiley, New York.

Shapiro, A.H. (1953). *The Dynamics and Thermodynamics of Compressible Fluid Flow*, Vol. 1, Wiley, New York.

Souli, M., Mahmadi, K., Aquelet, N. (2004). "ALE and Fluid Structure Interaction." Materials Science Forum, 465, 143-150.

Ugural A.C. (1981). *Stresses in Plates and Shells*, McGraw-Hill, New York.

TABLE CAPTIONS

FIGURE CAPTIONS

Table 1. Properties of air (at 288 Kelvin)

Material constant	Symbol	Numerical value	Units
Density	ρ	1.229	kg/m^3
Specific volume	ν	0.814	m^3/kg
Atmospheric pressure	P_0	0.1013	MPa
Viscosity	ω	1.73E-5	$N\sec/m^2$
Specific heat at constant volume	C_v	0.715	$kJ/(kg\ \ Kelvin)$
Ratio of specific heats	η	1.4	—

Table 2. Key finite element model components

Identifier	Type	Material	Entity	Finite element model (LS-DYNA)
Air (inside window)	Fluid	Air (compressible)	Eulerian solid	MAT_NULL, EOS_LINEAR_POLYNOMIAL
Air (outside window)	Fluid	Air (constant pressure)	Eulerian solid	MAT_NULL, EOS_LINEAR_POLYNOMIAL
Window frame	Structural	Steel	Solid	MAT_RIGID
Window frame plates	Structural	Steel	Shell	MAT_PLASTIC_KINEMATIC
Rubber membrane	Structural	Butyl rubber	Shell	MAT_BLATZ-KO_RUBBER
Window panel plates	Structural	Steel	Shell	MAT_PLASTIC_KINEMATIC
Glass window panels	Structural	Glass with polymer film	Shell	MAT_LAMINATED_GLASS
Window frame adhesive	Structural	Urethane adhesive	Constraint	CONTACT_TIED_SURFACE_TO_SURFACE
Window panel adhesive	Structural	Urethane adhesive	Constraint	CONTACT_TIED_SURFACE_TO_SURFACE

Table 3. Models analyzed in the design-parameter sensitivity study

System identification	Vent hole diameter	Vent area / AFRL vent area	Chamber thickness	Chamber thickness / AFRL chamber thickness
D0 / T6	No venting	0%	152 mm (6 in.)	100%
D0.75 / T6	19 mm (0.75 in.)	25%	152 mm (6 in.)	100%
D1.5 / T6 (AFRL)	38 mm. (1.5 in.)	100%	152 mm (6 in.)	100%
D2.5 / T6	64 mm (2.5 in.)	278%	152 mm (6 in.)	100%
D4.0 / T6	102 mm (4.0 in.)	711%	152 mm (6 in.)	100%
D1.5 / T10	38 mm (1.5 in.)	100%	254 mm (10 in.)	167%
D4.0 / T10	102 mm (4.0 in.)	711%	254 mm (10 in.)	167%

Table 4. Maximum membrane forces

System identification	Maximum shear force / Maximum AFRL shear force	Maximum resultant force / Maximum AFRL resultant force
D0 / T6	217%	275%
D1.5 / T6 (AFRL)	100%	100%
D1.5 / T10	67%	88%

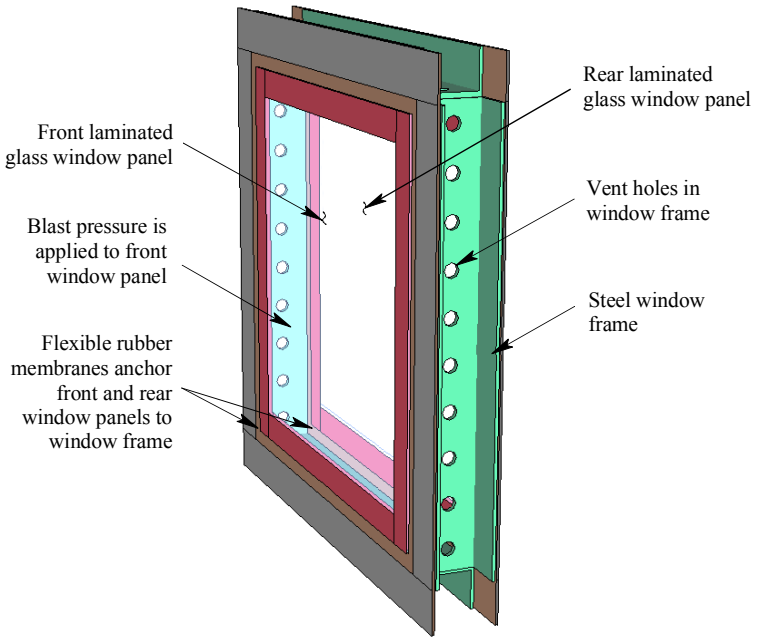

Figure 1. Blast-resistant AFRL flex-window system

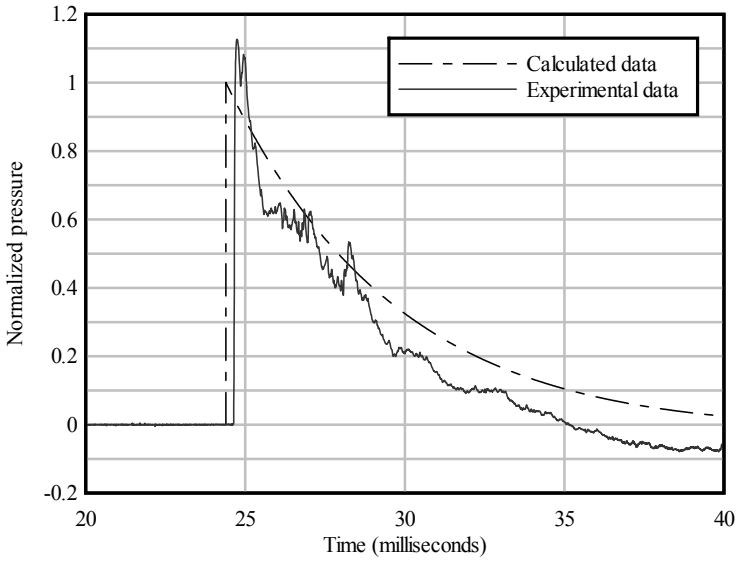

Figure 2. Comparison of calculated and experimentally measured air-blast pressure data

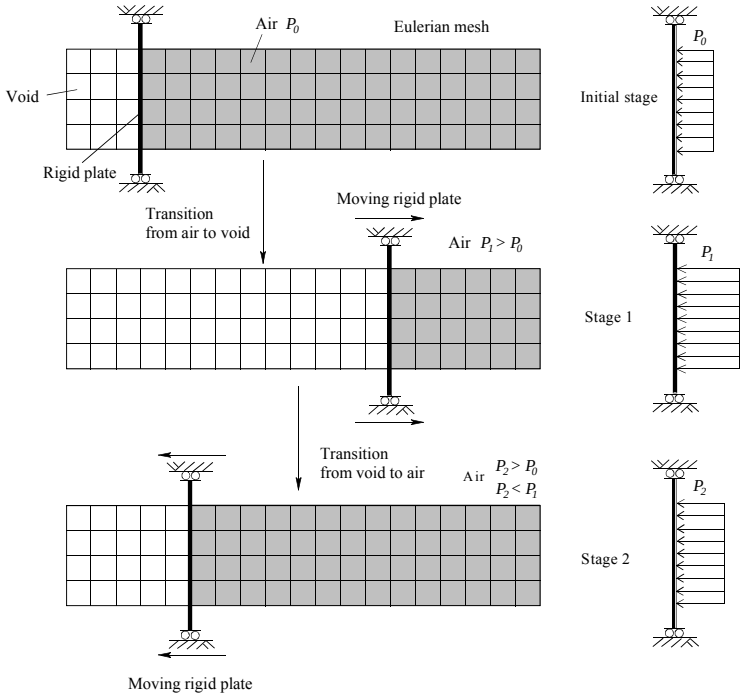

Figure 3. Conceptual model of fluid-structure interaction using the "single material and void" fluid element formulation

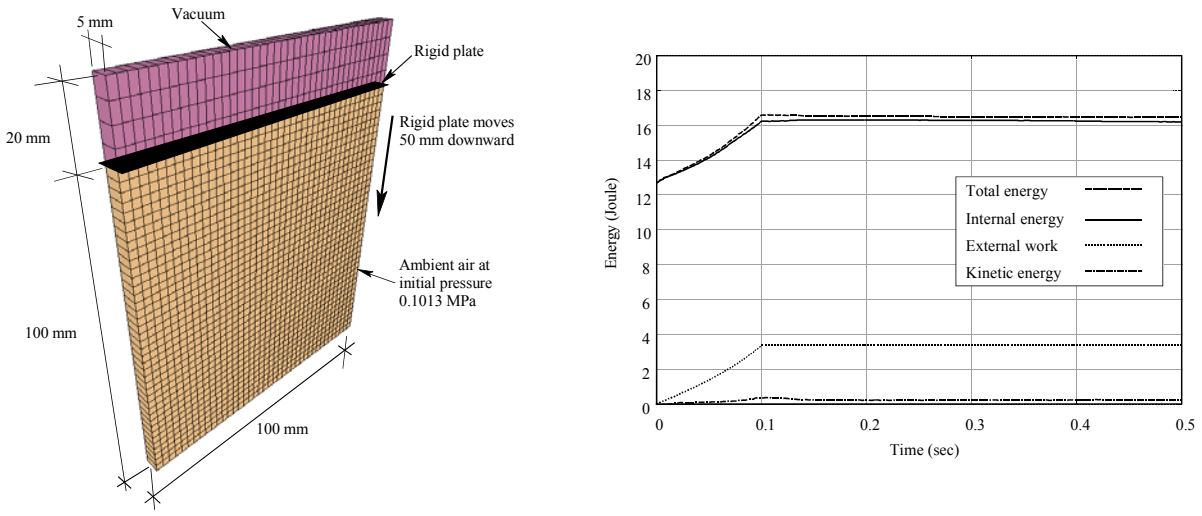

(a) Finite element model (b) Conservation of energy

Figure 4. Finite element simulation of compression

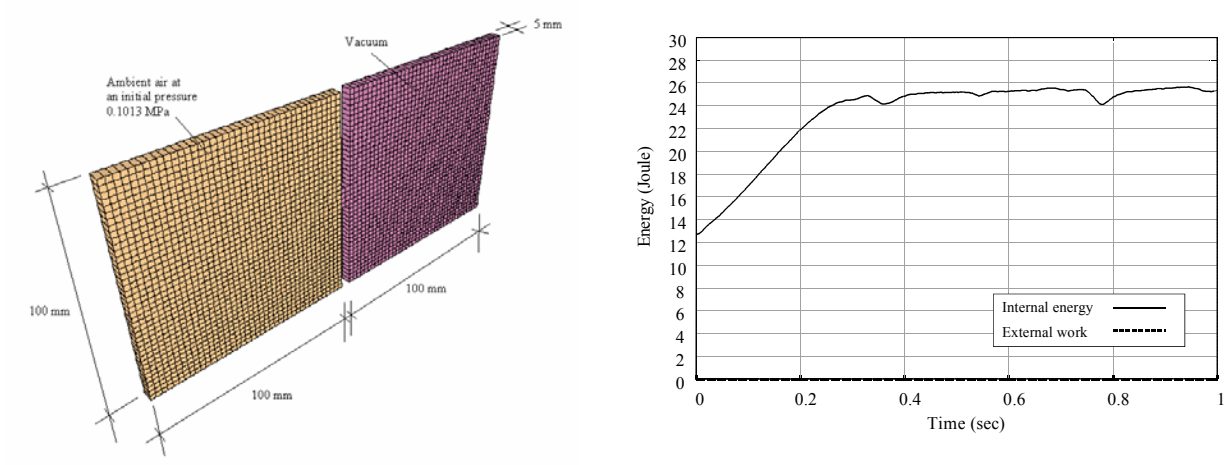

(a) Finite element model (b) Energy in free expansion process

Figure 5. Finite element model of expansion and flow of air

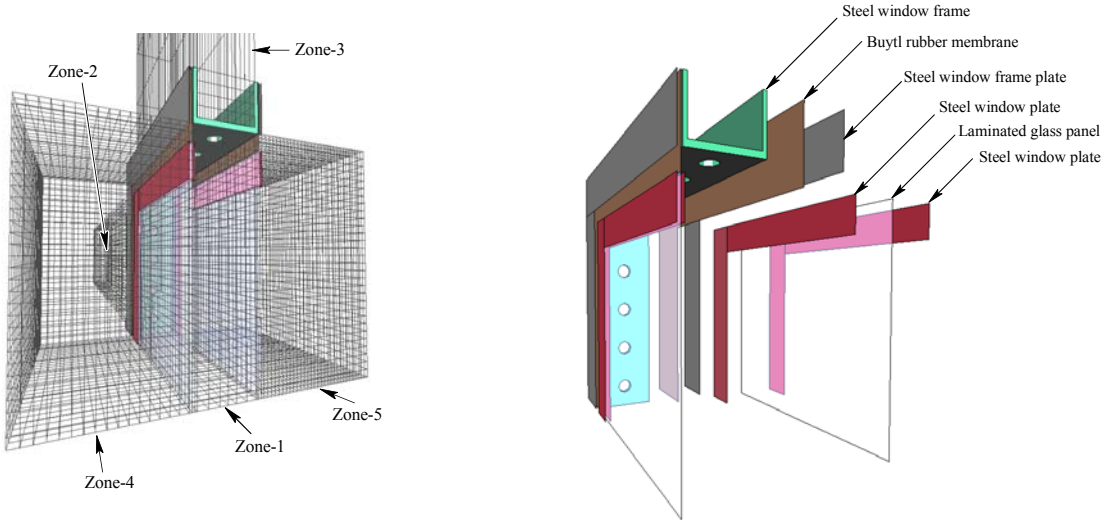

(a) Combined structure and fluid model

(b) Layering of structural components of Quarter symmetry model

Figure 6. Quarter symmetry finite element model

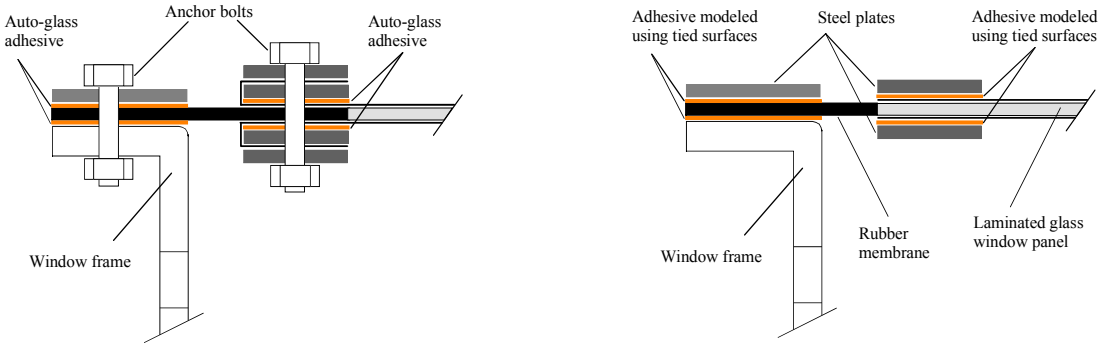

a) Physical system

b) Finite element model

Figure 7. Modeling the rubber membrane anchorage

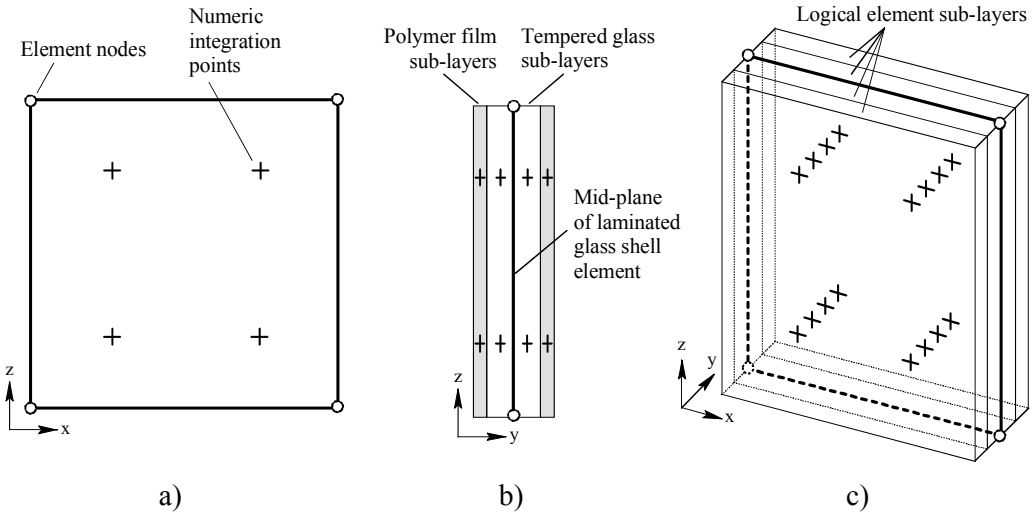

Figure 8. Modeling and failure of sub-layers within a glass laminate shell element

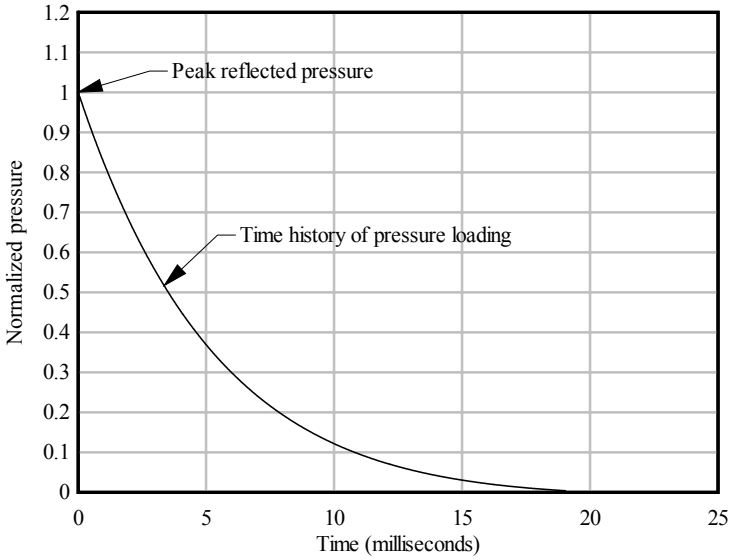

Figure 9. Normalized time history of blast pressure applied to front window panel of finite element model

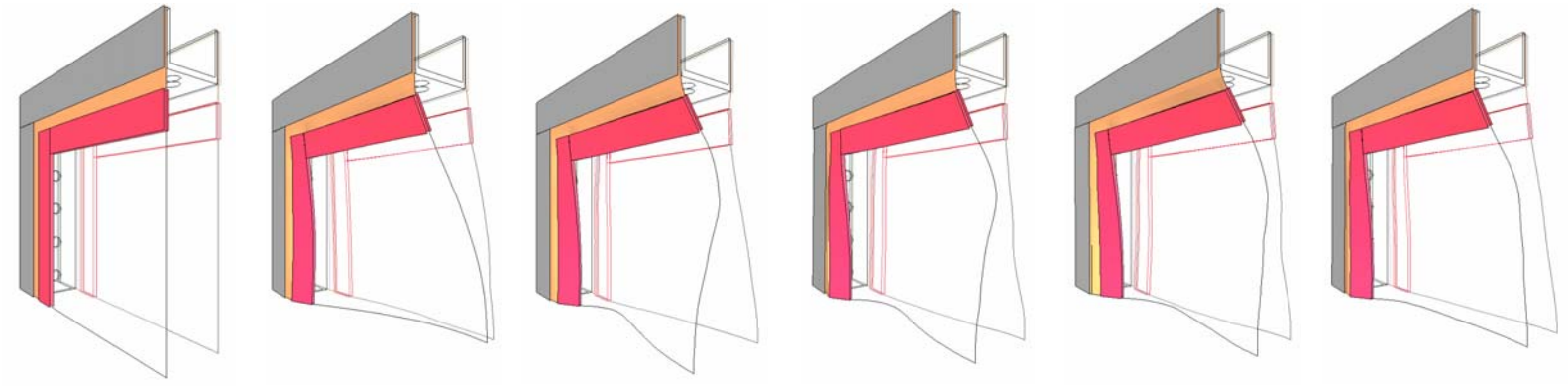

a) $t = 0$ msec b) $t = 10$ msec c) $t = 20$ msec d) $t = 30$ msec e) $t = 40$ msec f) $t = 50$ msec

Figure 10. Deflection response of front panel in simulation with fluid effects excluded

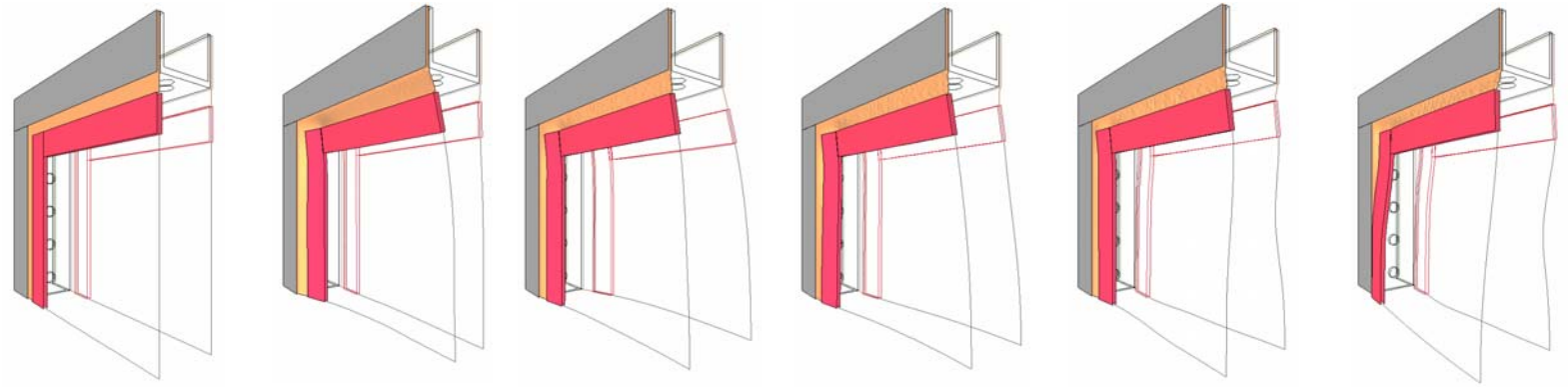

a) $t = 0$ msec b) $t = 10$ msec c) $t = 20$ msec d) $t = 30$ msec e) $t = 40$ msec f) $t = 50$ msec

Figure 11. Deflection response of rear panel in simulation with fluid effects included

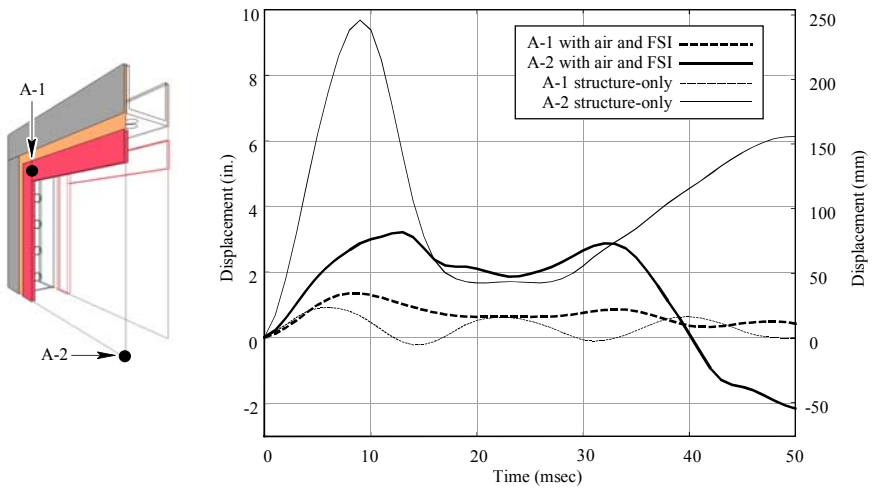

a) Front panel

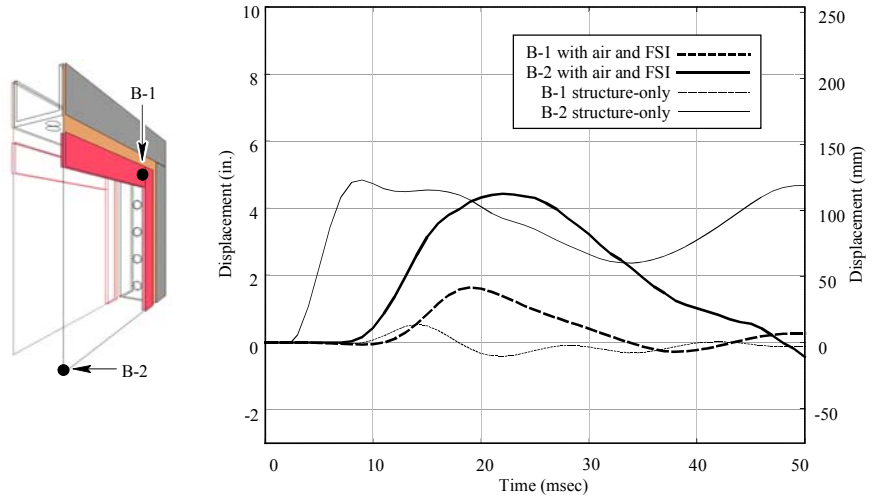

b) Rear panel

Figure 12. Predicted deflections of window panels

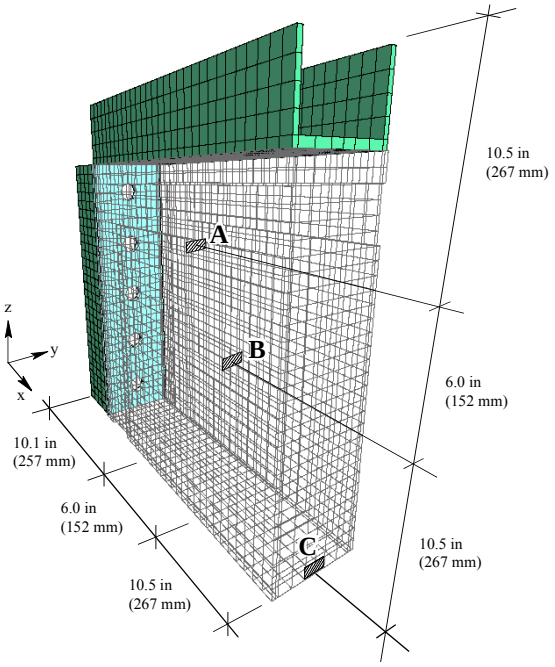

a) Locations of fluid pressure sampling locations

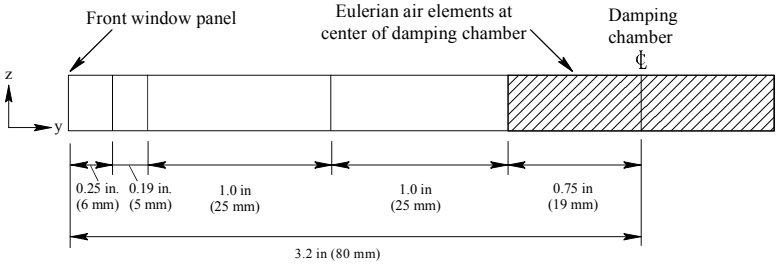

b) Partial cross-sectional view of chamber

Figure 13. Euler fluid elements used to evaluate internal chamber pressure

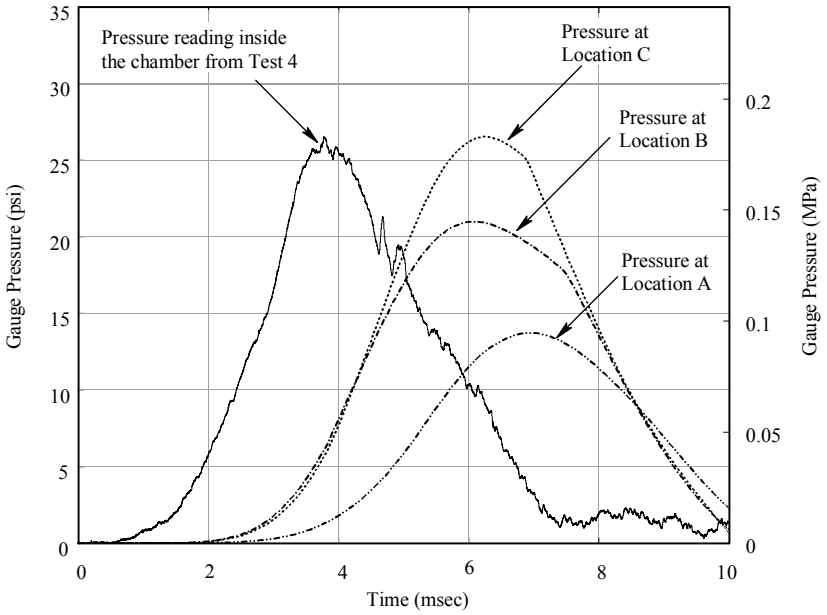

Figure 14. Internal window pressures measured experimentally and predicted numerically

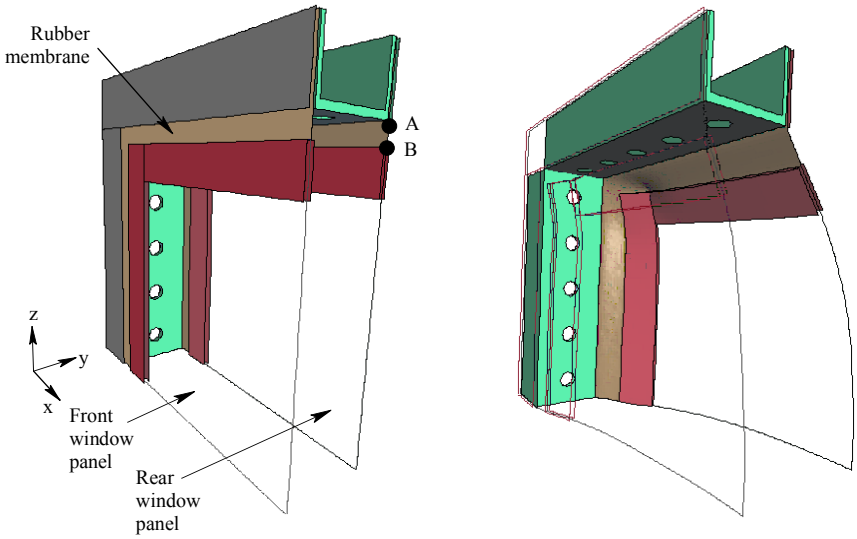

Figure 15. Elongation of the rear rubber membrane

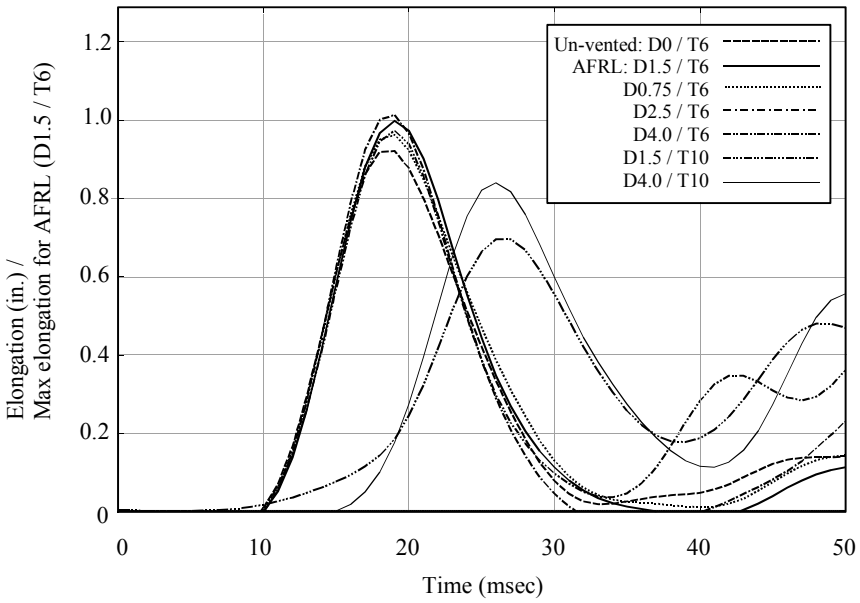

Figure 16. Normalized elongation of the rubber membrane during initial 50 msec duration